

Supporting Information for

Counterion Size and Nature Control Structural and Mechanical Response in Cellulose Nanofibril Nanopapers

Alejandro J. Benítez*, Andreas Walther

* (previously) DWI — Leibniz-Institute for Interactive Materials, Forckenbeckstr. 50, 52056 Aachen, Germany

Institute for Macromolecular Chemistry, Stefan-Meier-Str. 31, Albert-Ludwigs-University Freiburg, 79104 Freiburg, Germany.

& Freiburg Materials Research Center, Stefan-Meier-Str. 21, Albert-Ludwigs-University Freiburg, 79104 Freiburg, Germany.

& Freiburg Center for Interactive Materials and Bioinspired Technologies, Georges-Köhler-Allee 105, Albert-Ludwigs-University Freiburg, 79110 Freiburg, Germany.

E-mail: andreas.walther@makro.uni-freiburg.de

Thermoporosity Method	2
Nanopaper Preparation.....	4
pH-dependent Zeta Potential and Light Transmittance for CNF-Na⁺	5
Efficiency of Ion Exchange by Elemental Analysis.....	6
Mechanical Properties in this work.....	7
Second Yield Points.....	7
Literature Values for Ashby Plots.....	8
Cross sections of fractured CNF-Na⁺ at different RH.....	10
Nanostructure Characterization.....	11
Colloidal Properties of the Dispersions.....	12
DLVO Theory.....	13
Colloidal Stability during Salt Addition	15
Mechanical Properties of CNF bionanocomposites	16
References.....	17

Thermoporosity Method

This method consists in a series of isothermal melting steps of water within nanopores featuring size-dependent depressed melting temperatures. Generally, thermoporosimetry is applied for water-saturated pulps with nanopore diameters in the range 1.3–215.7 nm. The principle is to raise the temperature in a frozen sample to a value where it is held constant until the melting transition is completed. The melting of the sample is then repeated at a slightly higher temperature. The heat absorbed at each temperature is measured by integrating the endotherm. The melting heat correlates with the amount of molten water, and, consequently, the pore size distribution (PSD) is calculated from the melting temperature depression of the imbibed water. The relationship between pore diameter (D) and the melting temperature depression is described by the Gibbs-Thomson equation (Equation S1) and the correspondent values of temperature and pore diameter are listed in Table S1.^{1,2}

$$D = \frac{-4v_m T_0 \gamma_{1s}}{H_f(T_m - T_0)} \quad \text{Equation S1}$$

where v_m is the molar volume of ice ($19.6 \times 10^{-6} \text{ m}^3/\text{mol}$), T_0 is the melting temperature of water at normal pressure (273.15 K), γ_{1s} is the surface energy at the ice-water interface (12.1 mJ/m²), H_f is the specific heat of fusion of bulk water (334 J/g) and T_m is the melting temperature of a determined pore size (K).

The amount of non-freezing water (NFW) is calculated by subtracting the freezing water in the sample (total bound water or TBW and free water measured by heat) from the total water in the sample (determined gravimetrically).

$$\text{NFW} = \text{Total water (gravimetrically)} - \text{Freezing water (DSC)}$$

Table S1. Isothermal melting temperature and corresponding pore diameter given by Gibbs-Thomson in Equation S1.

$T_m \text{ } ^\circ\text{C}$	-33	-20	-17	-14	-11	-9	-7	-5	-3.5	-2.5	-1.6	-0.8	-0.4	-0.2
$D \text{ (nm)}$	1.3	2.2	2.5	3.1	3.9	4.8	6.2	8.6	12.3	17.3	27	53.9	107.9	215.7

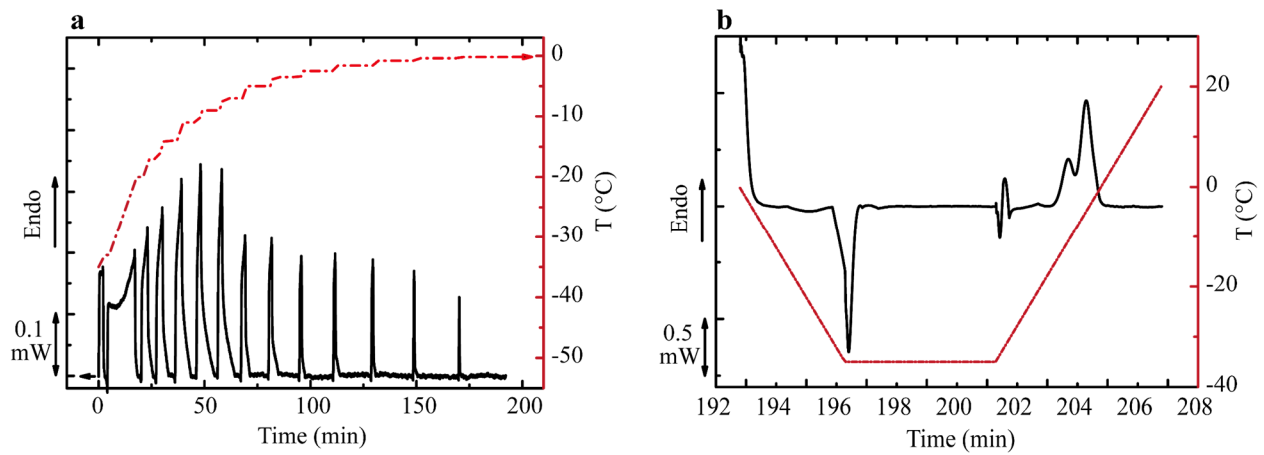


Figure S1. Thermoporosimetry for NFC- Na^+ as illustration. (a) Isothermal program for melting water within different pore sizes (0 to 193 min) and (b) dynamic scan as function of time (193-207 min) for total bound water determination.

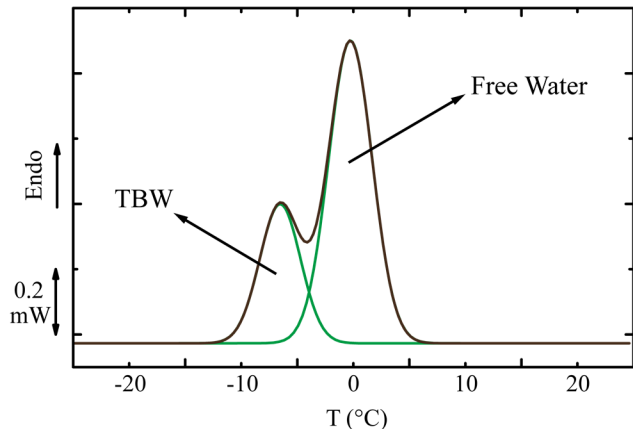


Figure S2. Calculation of the total freeze bound water. Overlapping peak corresponding to the melting of total freezing water and the deconvoluted areas corresponding to total freeze bound water (TBW) melting at low temperature inside the pores (left) and free water melting at high temperature (right) outside the nanopaper.

Nanopaper Preparation

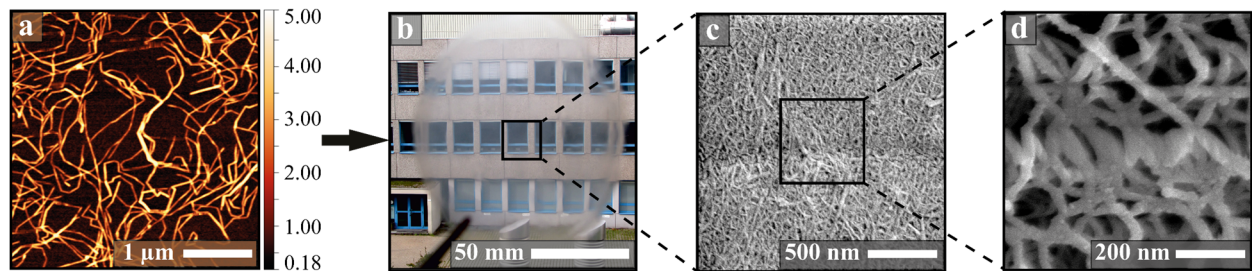


Figure S3. Structure of the CNF nanopapers. (a) AFM height image of CNFs, (c) transparent nanopaper obtained after vacuum filtration and (c-d) SEM micrographs of the top surface after sputter coating an Au/Pd layer.

pH-dependent Zeta Potential and Light Transmittance for CNF-Na⁺

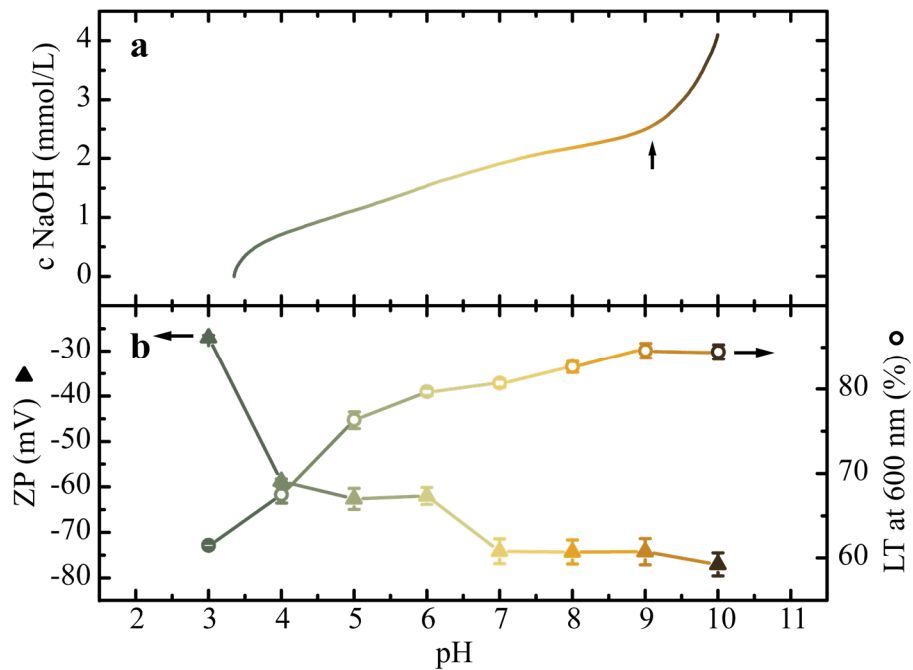


Figure S4. pH-dependent zeta potential and light transmittance for CNF-Na⁺ (0.25 wt%) when titrating from pH = 3 to pH = 10. (a) Titration of CNF-COOH (pH = 3) using NaOH to pH = 10. (b) Light transmittance (LT) at 600 nm and Zeta potential (ZP). The repulsion of the fibrils within the dispersions is increased by adding base improving the dispersion, increasing the LT up to 85% and reducing the ZP to -75 mV. From here, we select pH = 9 as the ideal point for the study with highest LT and ZP. pH = 10 requires larger amount of NaOH that could possibly produce solids after drying affecting the structure and mechanical response.

Efficiency of Ion Exchange by Elemental Analysis

Table S2. Elemental analysis of the different nanopapers

Nanopaper	Sodium Content ± 0.02 (mmol/g)	Corresponding counterion content ± 0.02 (mmol/g)
CNF-COOH	0.05 [#]	
CNF-Me⁺	Sodium Na ⁺	0.30
	Lithium Li ⁺	0.04 [#]
	Cesium Cs ⁺	0.04 [#]
CNF-QA⁺	Ammonium A ⁺	0.02 [#]
	Tetraethyl Ammonium TEA ⁺	0.03 [#]
	Tetrabutyl Ammonium TBA ⁺	0.03 [#]
	Tetrahexyl Ammonium THA ⁺	0.03 [#]

*Elemental analysis for cesium was not possible as the sensitivity of the detector is 3.3 g/L, and we estimate a content of 0.044 g/L (overall substitution ~0.30 mmol/g). The substitution is evidenced by EDX in Figure 1. [#]Trace amount of sodium can be found, partly influenced by sample preparation.

Mechanical Properties in this work

Table S3. Tensile properties of CNF nanopapers.

Nanopaper	E [GPa]	σ_y [MPa]	ε_y [%]	σ_b [MPa]	ε_b [%]	Ut [MJ/m ³]
CNF-COOH	10±3	98±6	1.2±0.6	210±10	10±1	11±1
Nanopapers with metal counterions (CNF-Me⁺)						
CNF-Li ⁺	18±2	143±10	0.9±0.2	301±30	9±1	16±2
CNF-Na ⁺	18±2	125±11	0.8±0.2	300±16	11±1	23±3
CNF-Cs ⁺	17±2	67±6	0.8±0.2	251±20	13±3	26±3
Nanopapers with alkyl-quaternized ammonium counterions (CNF-QA⁺)						
CNF-A ⁺	19±1	124±5	0.7±0.2	295±47	10±1	21±2
CNF-TEA ⁺	17±1	120±1	0.8±0.2	301±25	12±1	24±3
CNF-TBA ⁺	17±1	120±5	1.1±0.2	289±13	18±1	30±4
CNF-THA ⁺	16±2	105±5	1.7±0.3	272±15	21±2	38±5

Second Yield Points

Table S4. Overview over second yield points (σ_{y2} , ε_{y2}) for nanopapers with different counterions.

Nanopaper	σ_{y2} [MPa]	ε_{y2} [%]
CNF-COOH	-	-
Nanopapers with metal counterions (CNF-Me⁺)		
CNF-Li ⁺	-	-
CNF-Na ⁺	-	-
CNF-Cs ⁺	280±20	11±2
Nanopapers with alkyl-quaternized ammonium counterions (CNF-QA⁺)		
CNF-A ⁺	-	-
CNF-TEA ⁺	270±24	8±1
CNF-TBA ⁺	223±20	10±1
CNF-THA ⁺	245±22	15±2

Literature Values for Ashby Plots

Table S5. Mechanical properties of different studies correlated with the Ashby plots in Figure 3

Material Group	Name	Charge (mmol/g)	E (GPa)	ε_b (%)	σ_b (MPa)	U_t (MJ/m ³)	Ref	
CNF	CNF-COOH	0.44	10±1	10±1	210±10	11±1		
	CNF-Li ⁺		17±1	9±1	321±10	16±2		
	CNF-Na ⁺		18±1	11±1	300±10	23±3		
	CNF-Cs ⁺		17±1	13±3	251±10	26±3	Our work	
	CNF-A ⁺		19±1	10±1	283±10	21±2		
	CNF-TEA ⁺		11±1	12±1	301±10	24±3		
	CNF-TBA ⁺		11±1	18±1	289±10	30±4		
CNF (Green in Figure 3)	CNF-THA ⁺	0.54	11±1	21±2	272±10	38±5		
	CNF-Na ⁺		13±1	5.6±0.4	232±10	7±1	[3]	
	CNF- Na		10.0±0.5	8.0±0.4	290±15	15.0±0.8		
	CNF-A		9.0±0.5	10.0±0.5	225±13	17.0±0.9		
	CNF-TMA	1.7	8.5±0.4	14.0±0.7	240±12	25±1	[4]	
	CNF-TEA		6.0±0.3	18.0±0.9	150±8	22±1		
	CNF-TPA		6.0±0.3	8.0±0.4	130±7	8.0±0.4		
	CNF-TBA		6.0±0.3	12.0±0.6	140±7	14.0±0.7		
CNF (Green in Figure 3)	CNF-Fe ₃ ⁺	1.6	12±1	4.5±0.2	212±11	7.0±0.4		
	CNF-Al ₃ ⁺		16±1	3.3±0.2	252±13	6.0±0.3	[5]	
	CNF-Ca ₂ ⁺		13±1	3.8±0.2	195±10	5.0±0.3		
	CNF-Mg ₂ ⁺		15±1	6.0±0.3	277±14	11.0±0.6		
	CNF-Na (SC-CO ₂)		1.4±0.2	16.6±1	84±15	8±3		
	CNF-Na (L-CO ₂)		2.3	1.8±0.2	15±1	102±12	9±2	[6]
	CNF-Na (TER-B-FD)			5±0.4	8.8±0.4	120±3	7.3±0.3	
CNF (Green in Figure 3)	CNF-Na ⁺	0.575	1.4	10.8±0.5	7.5±0.4	223±12	12±0.6	[7]
	CNF-Na			14.6±0.7	7±2	227±26	11±4	[8]
	CNF-Na			13±1	7±1	202±20	10±3	[9]
	CNF-Na ⁺		0.44	16±2	5.7±0.6	213±13	6±1	[10]
	CNF DP-1100			13.2±0.6	10±1	214±7	15±2	
	CNF DP-820	0.515		10.4±0.5	7±1	181±12	9±2	[11]
	CNF DP-580			10.7±1	6±1	159±16	7±3	
	CNF DP-410			13.7±0.3	3.3±0.4	129±8	3.0±0.5	

Table S5. Cont. Mechanical properties of different studies correlated with the Ashby plots in Figure 3

Material Group	Name	Charge (mmol/g)	E (GPa)	ε_b (%)	σ_b (MPa)	U_t (MJ/m ³)	Ref
CNF/Polymer composites (Green in Figure 3)	CNF/PAM 75/25	1.4	12.9±0.6	5.0±0.3	255±13	9±0.5	[7]
	CNF/PVA 75/25		11.0±0.5	7.0±0.4	210±11	10±0.5	
	CNF/Starch 75/25	1.4	11.1±0.5	5.0±0.3	230±12	7.5±0.4	[12]
	CNF/AP 85/15		13.2±0.1	10±1	252±18	16±3	
	CNF/AP 82/18	1.4	13.4±0.3	9±2	240±23	15±4	[8]
	CNF/AP 77/23		13.6±0.2	8±2	221±17	12±3	
	CNF/XG 69/31	1.4	13±0.3	6±1	164±19	6±2	[13]
	CNF/GCL/AP 70/15/15		6.2±0.2	8.1±0.9	160±8	9±2	
	CNF/GCL/AP 60/20/20	1.4	4.8±0.2	9.3±0.5	120±5	7.8±0.5	[14]
	CNF/GCL/AP 50/25/25		4.3±0.1	11.0±0.6	80±3	6.5±0.8	
	CNF/GCL/AP 40/30/30		3.1±0.1	15±1	58±5	6.2±0.8	
CNF/PB-b-PDMAEMAq (Green in Figure 3)	CNF/PB-b-PDMAEMAq 91/9		10±1	4.5±0.9	166±13	6±1	
	CNF/PB-b-PDMAEMAq 83/17	0.575	11±1	2.4±0.5	145±16	2.5±0.8	[9]
	CNF/PB-b-PDMAEMAq 71/29		7.3±1	9.1±0.7	165.2±21	11±2	
	CNF/PB-b-PDMAEMAq 50/50		6.2±0.2	4.6±0.5	96±1	3.3±0.5	
CNF-Na/EG _x DMAm _y (Purple in Figure 3)	CNF-Na/DMAm 50/50		9±1	5.8±0.5	125±8	4±1	
	CNF-Na/EG ₂₁ DMAm ₇₉ 50/50		4.7±0.3	17±1	86±7	8±2	
	CNF-Na/EG ₅₄ DMAm ₄₆ 50/50	0.44	3.4±0.5	26±2	69±5	11±1	[10]
	CNF-Na/EG ₇₂ DMAm ₂₈ 50/50		4±1	22±5	74±8	10±1	
	CNF-Na/EG 50/50		4±1	17±1	75±4	8±1	
CNF/HEC (Magenta in Figure 3)	CNF/HEC 54/28		8.2±0.6	14±1	202±5	20±2	
	CNF/HEC 31/56	0.575	4.6±0.5	24±3	147±6	27±4	[15]
	CNF/HEC 8/64		1.9±0.2	33±2	66	15±1	
CNF/Clay (Blue in Figure 3)	CNF/MTM 5		18±1	7.6±0.4	509±15	26±5	
	CNF/MTM 10	1.21	18±1	5.8±0.8	453±20	17±6	[16]
	CNF/MTM 25		20±1	4.7±0.8	439±20	14±3	
	CNF/MTM 50		19±1	4.3±0.2	420±20	10.9±0.2	
	MTM/CNF/PVA 35/35/30		22±2	2.0±0.2	302±30	3.7±0.4	[17]
	CNF/Sap 10		15±1	10±2	425±39	30±6	
	CNF/Sap 25	1.2	22±2	7±2	375±56	18±7	[18]
	CNF/Sap 50		22±4	4.3±0.7	339±20	11±2	

Cross sections of fractured CNF-Na⁺ at different RH

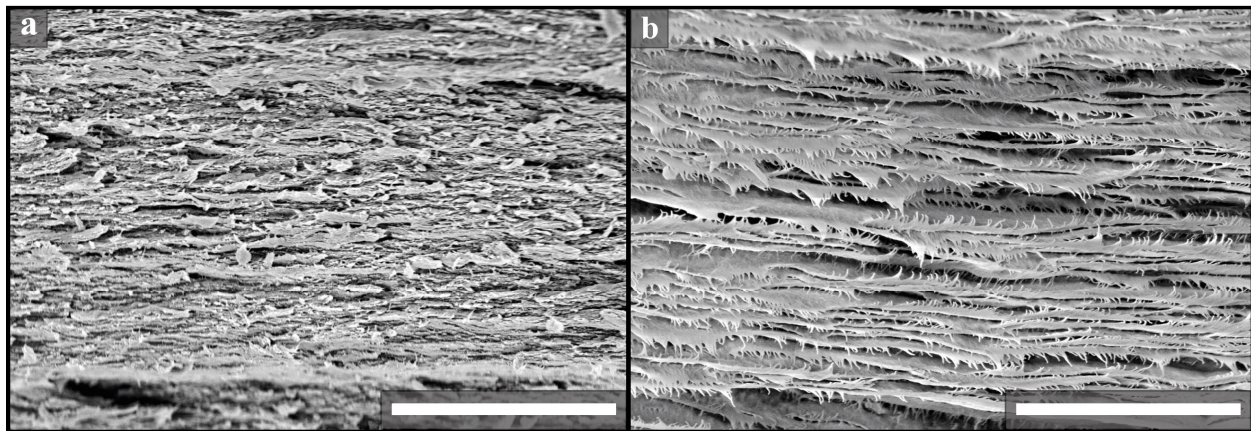


Figure S5. Cross section micrographs of fractured CNF-Na⁺ nanopapers at different relative humidities (RH): (a) 20% and (b) 99%. Scale bars are 5 μm.

Nanostructure Characterization

Table S6. Nanostructure parameters for CNF nanopapers. Counterion size, specific surface area (SSA) measured by Kr adsorption, apparent density (ρ), water content by humidity sorption and thermoporosimetry parameters.

Nanopaper	Ion Radius (nm) [#]	SSA (m ² /g)	ρ (g/cm ³)	Humidity Sorption			Thermoporosity	
				Water Content (%)			NFW* (g _{H2O} /g _{dry} CNF)	TBW* (g _{H2O} /g _{dry} CNF)
				RH 5%	RH 50%	RH 95%		
COOH	-	0.17±0.01	1.36±0.02	0.55±0.06	8±1	19±2	0.45±0.06	0.45±0.07
CNF-Li ⁺	0.076	0.049±0.06	1.41±0.03	0.70±0.09	10±1	25±2	0.44±0.06	0.12±0.06
CNF-Na ⁺	0.102	0.039±0.05	1.42±0.03	0.60±0.06	11±1	27±3	0.42±0.05	0.20±0.05
CNF-Cs ⁺	0.167	0.042±0.05	1.43±0.03	0.34±0.03	11±1	26±3	0.46±0.05	0.28±0.05
CNF-A ⁺	0.143	0.043±0.02	1.42±0.03	0.33±0.03	9±1	26±3	0.43±0.05	0.06±0.05
CNF-TEA ⁺	0.343	0.045±0.09	1.42±0.03	0.35±0.04	10±1	24±2	0.46±0.05	0.19±0.05
CNF-TBA ⁺	0.415	0.043±0.08	1.42±0.03	0.45±0.03	10±1	26±3	0.46±0.06	0.23±0.08
CNF-THA ⁺	0.552	0.041±0.07	1.41±0.03	0.42±0.05	9±1	23±2	0.44±0.05	0.30±0.05

* Non-freeze bound water (NFW) and total freeze bound water (TBW).

The ionic radius for the counterions were taken from literature,¹⁹⁻²¹ except for tetrahexyl ammonium (THA), for which we estimate the ionic size by a linear extrapolation of the known quaternized tetraalkyl ammoniums with different substituents (methyl, ethyl, propyl and butyl).

Colloidal Properties of the Dispersions

Table S7. Zeta Potential (ZP), Light Transmittance at 600 nm wavelength (LT) and maximal Potential (V) from DLVO theory of Cross-Cylinders for CNF dispersions. CNF dispersions have a concentration of 0.25 wt%

Dispersion	Counterion	ZP (mV)	LT at 600 nm (%)	V ($k_B T$) (max. at H~0.3 nm)
CNF-COOH (pH = 3)	-	-27±1	71.5±0.1	1.6
CNF-Me ⁺ (pH = 9)	Li ⁺	-74±2	84.2±0.7	8.8
	Na ⁺	-74±3	84.6±0.7	8.9
	Cs ⁺	-78±2	86.4±0.3	9.5
CNF-QA ⁺ (pH = 9)	A ⁺	-71±2	84.5±0.8	8.2
	TEA ⁺	-77±3	85.1±0.4	9.3
	TBA ⁺	-80±3	87.1±0.8	9.8
	THA ⁺	-87±1	89.2±0.3	11.0

DLVO Theory

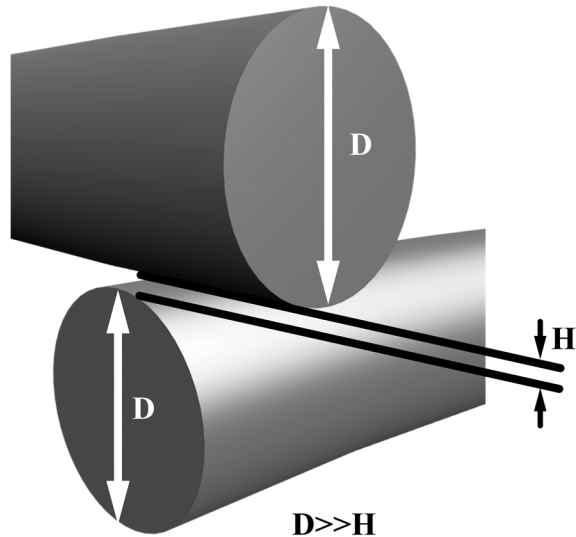


Figure S6. Crossed CNF model for DLVO theory. D is the diameter and H is the distance between the of the nanofibers. ($D/2 \gg H$)

DLVO theory calculation for cylindrical rods: total interaction potential energy (V , Equation S2).²²
Diameter, D , = 2.25 from height average in AFM.¹⁰

$$V = V_R + V_A \quad \text{Equation S2}$$

Here, V_R (Equation S3) is the repulsive energy from an electric double layer repulsion and V_A (Equation S5) correspond to the attraction Van der Waals energy.

$$V_R = 64\pi \frac{D}{\kappa^2} n k_B T \gamma^2 e^{-\kappa H} \quad \text{Equation S3}$$

$$\gamma = \tanh\left(\frac{\psi_0}{102.75}\right) \quad [\text{J} \cdot \text{m}^{-1}] \text{ at } 25^\circ\text{C} \quad \text{Equation S4}$$

$$V_A = \frac{-AD}{12H} \quad \text{Equation S5}$$

$$\kappa = \sqrt{\frac{2c_0e^2}{\epsilon_0\epsilon kT}} \quad \text{Equation S6}$$

where n is the number of density of ions ($n = c_0 * N_a$), c_0 is the initial concentration of ions (2.5 mmol/L \sim 1 mmol/gCNF), N_a is the Avogadro's number, k_B is the Boltzmann constant, T is the absolute temperature, γ is an interaction constant simplified for a monovalent system of ions (Cation/Anion ration of 1:1, Equation S4), ψ_0 is the surface potential of the particles approximated to the measured Zeta Potential, A is the Hamaker constant for cellulose surfaces (3.5×10^{-21} J)²³, H is the distance between the particles, κ correspond to the Debye length (Equation S6), e is the electron charge, ϵ_0 is the vacuum permittivity and ϵ is the relative permittivity.

Colloidal Stability during Salt Addition

Table S8. Zeta Potentials (ZP) for CNF dispersion/salt systems with different concentration of salt.

Counterion Type	Dispersion/Salt System	ZP (mV)		
		0 mmol/L	75 mmol/L	170 mmol/L
Me^+	CNF-Li ⁺ /LiCl	-74±2	-37±2	-27±1
	CNF-Na ⁺ /NaCl	-74±3	-44±3	-30±1
	CNF-Cs ⁺ /CsCl	-78±2	-44±1	-30±3
QA^+	CNF-A ⁺ /ACl	-71±2	-42±1	-30±2
	CNF-TEA ⁺ /TEACl	-77±3	-51±1	-33±1
	CNF-TBA ⁺ /TBACl	-80±3	-63±3	-36±2
	CNF-THA ⁺ /THACl	-87±1	-10±4	-7±1

The results show that the hydrophobicity given by the hexyl chains has a strong concentration dependent influence. At low concentration (no salt) CNF-THA⁺ has the highest ZP, yet addition of THACl salt leads to a quick disruption of electrostatic stabilization (Table S8). THACl salt has a solubility limit of ca. 0.05 mol/L at 25 °C. The CNF-THA⁺ dispersion could not be used for further aggregation and sedimentation speed analysis due to precipitation (Figure S7).



Figure S7. Dispersions of CNF-THA+/THACl at different salt content. Strong coagulation at early stages is observed. THACl salt has a solubility limit of ~0.05 mol/L at 25 °C. The CNF content is 0.25 wt%.

Mechanical Properties of CNF bionanocomposites

Table S9. Tensile properties of CNF/polymer bionanocomposites.

Bionanocomposite	E [GPa]	σ_y [MPa]	ε_y [%]	σ_b [MPa]	ε_b [%]	U_t [MJ/m ³]
CNF-Na ⁺ /EG ₅₄ DMAm ₄₆	3.4±0.5	23±6	0.8±0.2	69±5	26±2	11±1
CNF-A ⁺ /EG ₅₄ DMAm ₄₆	2.8±0.2	21±1	1.5±0.2	63±2	39±3	22±1
CNF-TBA ⁺ /EG ₅₄ DMAm ₄₆	0.9±0.1	10±1	1.2±0.2	44±2	59±3	17±1

References

1. Luukkonen, P.; Maloney, T.; Rantanen, J.; Paulapuro, H.; Yliruusi, J. *Pharm. Res.* **2001**, *18*, 1562-1569.
2. Orsolini, P.; Michen, B.; Huch, A.; Tingaut, P.; Caseri, W. R.; Zimmermann, T. *ACS Appl. Mater. Interfaces* **2015**, *7*, 25884-25897.
3. Benítez, A. J.; Torres-Rendon, J. G.; Poutanen, M.; Walther, A. *Biomacromolecules* **2013**, *14*, 4497-4506.
4. Shimizu, M.; Saito, T.; Fukuzumi, H.; Isogai, A. *Biomacromolecules* **2014**, *15*, 4320-4325.
5. Shimizu, M.; Saito, T.; Isogai, A. *J. Membr. Sci.* **2016**, *500*, 1-7.
6. Sehaqui, H.; Zhou, Q.; Ikkala, O.; Berglund, L. A. *Biomacromolecules* **2011**, *12*, 3638-3644.
7. Kurihara, T.; Isogai, A. *Cellulose* **2014**, *21*, 291-299.
8. Prakobna, K.; Galland, S.; Berglund, L. A. *Biomacromolecules* **2015**, *16*, 904-912.
9. Wang, M.; Olszewska, A.; Walther, A.; Malho, J.-M.; Schacher, F. H.; Ruokolainen, J.; Ankerfors, M.; Laine, J.; Berglund, L. A.; Österberg, M.; Ikkala, O. *Biomacromolecules* **2011**, *12*, 2074-2081.
10. Benítez, A. J.; Lossada, F.; Zhu, B.; Rudolph, T.; Walther, A. *Biomacromolecules* **2016**, *17*, 2417-2426.
11. Henriksson, M.; Berglund, L. A.; Isaksson, P.; Lindström, T.; Nishino, T. *Biomacromolecules* **2008**, *9*, 1579-1585.
12. Kurihara, T.; Isogai, A. *Cellulose* **2015**, *22*, 2607-2617.
13. Prakobna, K.; Terenzi, C.; Zhou, Q.; Furó, I.; Berglund, L. A. *Carbohydr. Polym.* **2015**, *125*, 92-102.
14. Svagan, A. J.; Azizi Samir, M. A. S.; Berglund, L. A. *Biomacromolecules* **2007**, *8*, 2556-2563.
15. Sehaqui, H.; Zhou, Q.; Berglund, L. A. *Soft Matter* **2011**, *7*, 7342-7350.
16. Wu, C.-N.; Saito, T.; Fujisawa, S.; Fukuzumi, H.; Isogai, A. *Biomacromolecules* **2012**, *13*, 1927-1932.
17. Wang, J.; Cheng, Q.; Lin, L.; Jiang, L. *ACS Nano* **2014**, *8*, 2739-2745.
18. Wu, C.-N.; Yang, Q.; Takeuchi, M.; Saito, T.; Isogai, A. *Nanoscale* **2014**, *6*, 392-399.
19. Shannon, R. *Acta Cryst. A* **1976**, *32*, 751-767.
20. Conway, B. E.; Ayrancı, E. *J. Solution Chem.* **1999**, *28*, 163-192.
21. Marcus, Y. Ion Properties. In *Encyclopedia of Applied Electrochemistry*, Kreysa, G.; Ota, K.-i.; Savinell, R. F., Eds. Springer New York: New York, NY, 2014; pp 1101-1106.
22. Israelachvili, J. N. *Intermolecular and Surface Forces (Third Edition)*. Elsevier: San Diego, 2011; p 253-340.
23. Notley, S. M.; Pettersson, B.; Wågberg, L. *J. Am. Chem. Soc.* **2004**, *126*, 13930-13931.